



Application of machine learning to the prediction of the boiling heat transfer coefficient of R32 inside a multiport mini-channel tube

Nurlaily Agustiarini¹ · Hieu Ngoc Hoang¹ · Jong-Taek Oh¹ · Normah Mohd-Ghazali²

Received: 26 April 2022 / Accepted: 24 August 2022 / Published online: 31 October 2022
 © Akadémiai Kiadó, Budapest, Hungary 2022

Abstract

The possibility of using machine learning to predict the heat transfer coefficient is becoming more evident. In fact, artificial neural networks (ANN) are widely used in heat transfer coefficient research. In this study, an ANN was used in the dataset training and testing of the boiling heat transfer coefficient of R32 inside a horizontal multiport mini-channel tube with a hydraulic diameter of 0.969 mm and an aspect ratio of 0.6. A mass flux range of 50–500 kg m⁻² s⁻¹, heat flux of 3–6 kW m⁻², saturation temperature of 6 °C, and vapor quality up to 1 were applied as experimental conditions. The superposition, asymptotic, and flow pattern models were used to assess the experimental data. The ANN model with hidden layers (96,72,48,24) and 16 input parameters (Re_{vo}, Re_{lo}, Bd, Fr_{vo}, We_{vo}, Fr_{lo}, We_{lo}, Re_v, Fr_v, Re_l, We_l, Pr_v, X_{tt}, Co, Pr_l, and Bo) was included in the prediction of the boiling heat transfer coefficient of R32 inside a horizontal multiport mini-channel tube and achieved better results than the empirical correlation models with a mean deviation of 6.35%. Results indicate that ANN models can be applied to improve the prediction accuracy of the boiling heat transfer coefficient, especially in multiport mini-channel tubes.

Keywords Machine learning · ANN · Boiling heat transfer coefficient · R32 · Mini-channel tube

List of symbols

d_h	Hydraulic diameter (mm)	Ga	Galileo number, $Ga = \frac{\rho_l g (\rho_l - \rho_v) d^3}{\mu_l}$
Bd	Bond number, $Bd = \frac{g(\rho_l - \rho_v) D_h^2}{\sigma}$	h	Heat transfer coefficient (kW m ⁻² K ⁻¹)
Bo	Boiling number, $Bo = \frac{\sigma}{G h_{fg}}$	i	Enthalpy (J kg ⁻¹)
Co	Convection number, $Co = \left(\frac{1-x}{x}\right)^{0.8} \left(\frac{\rho_l - \rho_v}{d}\right)$	Ja	Jakob number, $Ja = cp_l \frac{(T_w - T_{sat})}{h_{fg}}$
Cp	Specific heat (J kg ⁻¹ °C ⁻¹)	Ka	Kapitza number, $Ka = \frac{\mu_l^4 g}{\rho_l \sigma^3}$
Fa	Fang number, $Fa = \frac{(\rho_l - \rho_v) \sigma}{G^2 d}$	k_l	Thermal conductivity of liquids (W m ⁻¹ K ⁻¹)
Fr _l	Liquid Froude number, $Fr_l = \frac{[G(1-x)]^2}{\rho_l^2 g D_h}$	k_v	Thermal conductivity of vapor (W m ⁻¹ K ⁻¹)
Fr _{lo}	Liquid-only Froude number, $Fr_{lo} = \frac{G^2}{\rho_l^2 g D_h}$	L	Length (m)
Fr _v	Vapor Froude number, $Fr_v = \frac{(Gx)^2}{\rho_v^2 g D_h}$	m	Mass flow rate (kg s ⁻¹)
Fr _{vo}	Vapor-only Froude number, $Fr_{vo} = \frac{G^2}{\rho_v^2 g D_h}$	Nu _{tp}	Two-phase Nusselt number, $Nu_{tp} = \frac{hL}{k_l}$
G	Mass flux (kg m ⁻² s ⁻¹)	Pr _l	Liquid Prandtl number, $Pr_l = \frac{\mu_l c_{p_l}}{k_l}$
		Pr _v	Vapor Prandtl number, $Pr_v = \frac{\mu_v c_{p_v}}{k_v}$
		P_{sat}	Saturation pressure (MPa)
		q	Heat flux (kW m ⁻²)
		Q	Heat transfer rate (W)
		R^2	The coefficient of determination
		Re _l	Liquid Reynold number, $Re_l = \frac{G(1-x)D_h}{\mu_l}$
		Re _{lo}	Liquid-only Reynold number, $Re_{lo} = \frac{GD_h}{\mu_l}$
		Re _v	Vapor Reynold number, $Re_v = \frac{GxD_h}{\mu_v}$
		Re _{vo}	Vapor-only Reynold number, $Re_{vo} = \frac{GD_h}{\mu_v}$
		Su _l	Liquid Suratman number, $Su_l = \frac{\sigma \rho_l D_h}{\mu_l^2}$

✉ Jong-Taek Oh
 ohjt@chonnam.ac.kr

¹ Department of Refrigeration and Air-Conditioning Engineering, Graduate School, Chonnam National University, Yeosu 59626, South Korea

² School of Mechanical Engineering, Faculty Engineering, Universiti Teknologi Malaysia, 81310 Johor Bahru, Johor, Malaysia

Su_v	Vapor Suratman number, $Su_v = \frac{\sigma \rho_v D_h}{\mu_v^2}$
T_{sat}	Saturation temperature (°C)
T_w	Wall temperature (°C)
We_l	Liquid Weber number, $We_l = \frac{[G(1-x)]^2 D_h}{\rho_l \sigma}$
We_{lo}	Liquid-only Weber number, $We_{lo} = \frac{G^2 D_h}{\rho_l \sigma}$
We_v	Vapor Weber number, $We_v = \frac{(Gx)^2 D_h}{\rho_v \sigma}$
We_{vo}	Vapor-only Weber number, $We_{vo} = \frac{G^2 D_h}{\rho_v \sigma}$
x	Vapor quality
X_{tt}	Lockhart–Martinelli parameter, $X_{tt} = \left(\frac{1-x}{x}\right)^{0.9} \left(\frac{\rho_v}{\rho_l}\right)^{0.5} \left(\frac{\mu_l}{\mu_v}\right)^{0.1}$

Greek letters

α	Void fraction
μ	Viscosity (Pa s)
δ	Thickness (m)
ρ	Density (kg m ⁻³)
σ	Surface tension (N m ⁻¹)

Subscripts

cb	Convective boiling
Exp	Experimental
in	Inlet
nb	Nucleate boiling
out	Outlet
Pred	Prediction
ref	Refrigerant
sat	Saturation
tp	Two-phase
l	Liquid
lo	Liquid-only
loss	Losses
v	Vapor
vo	Vapor-only
W	Wall

Introduction

Boiling heat transfer coefficient correlation

The heat transfer coefficient is an important factor in the design of heat exchangers for refrigeration and air-conditioning systems. There have been many studies on the prediction of the boiling heat transfer coefficient. The well-known correlation to predict the boiling heat transfer coefficient by Chen [1] in 1966 introduced the suppression factor S on the nucleate boiling term and enhancement factor F on the convective boiling term. Since then, the Chen correlation has been used as a basis for the calculation of the superposition model, asymptotic model, and flow pattern model.

Gungor and Winterton [2], Jung et al. [3], Li et al. [5], and Mahmoud and Karayiannis [4] proposed superposition models by modifying the suppression factor and enhancement factor according to their experimental data to improve the prediction accuracy.

Gungor and Winterton [2] modified the enhancement factor and suppression factor with the Froude number $Fr < 0.5$, particularly for a horizontal tube with a hydraulic diameter of 2.95–32 mm. The proposed correlation for saturated boiling resulted in a mean deviation of 21.4%. Jung et al. [3] proposed a boiling heat transfer coefficient for refrigerant mixtures in a stainless steel tube with an inner diameter of approximately 9 mm and achieved a mean deviation of approximately 7.2% for pure refrigerant and 9.6% for mixed refrigerants. However, both correlations by Gungor and Winterton [2] and Jung et al. [3] did not include alternative refrigerants and the mini-channel tube was not within their tube ranges. In 2013, Li et al. [5] and Mahmoud and Karayiannis [4] also proposed a modified version of Chen's correlation with mean deviations of 14.3% and 20%, respectively. However, the mean deviation of these correlations is still not sufficiently low, indicating that a good prediction will not be achieved in different experimental conditions.

In 1961, Kutateladze [6] introduced a “power type” addition in the modification to the nucleate boiling and convective boiling terms to predict the heat transfer coefficient. Liu and Winterton [7] proposed a boiling heat transfer coefficient correlation in which the enhancement factor for the convective boiling and suppression factor for the nucleate boiling included the Prandtl number and that resulted in a 20.5% mean deviation for approximately 10 working fluids in total. Steiner and Taborek [8] also applied an asymptotic model to the boiling heat transfer correlation with a “power type” addition of 3 ($n = 3$). However, the suppression factor for the nucleate boiling term is not included in this correlation and only the enhancement factor for the convective boiling term is considered, which is a function of vapor quality and density ratio. Their proposed asymptotic model could predict the boiling heat transfer coefficient in a vertical tube with a 20% to 30% mean deviation. Wattelet et al. [9] proposed the heat transfer coefficient correlation with “power type” addition of 2.5 ($n = 2.5$) which developed using wavy-stratified flow annular flow data from R134a and R12 with mean deviations lower than 10%. A Froude number was included to the convective boiling side represented the wavy-stratified flow. Tapia and Ribatski [10] proposed an asymptotic correlation by taken the same “power type” addition as Liu and Winterton [7] and produced low mean deviation by modified Kanizawa et al. (2016) correlation. Again, a lower mean deviation would produce a higher accuracy for the prediction of the boiling heat transfer coefficient, a result of which the abovementioned asymptotic models could not give an accurate prediction to other experimental data due to uncertain

“power type” value of each correlation. Particularly, each experimental data needs its own prediction model.

With the combination of asymptotic models and flow pattern analysis to predict a heat transfer coefficient, Kattan–Thome–Favrat [11] proposed a flow pattern model in 1998. This model is based on the flow regime in a horizontal tube and includes partial tube wall wetting and partial tube dryout in an annular flow, producing results with mean a deviation of 13.3%. A similar method was applied to the heat transfer coefficient correlation proposed by Thome and El Hajal [12] with CO₂ (carbon dioxide) as the working fluid. With 404 data points for hydraulic diameters between 0.79 and 10.06 mm, an accurate prediction of the heat transfer coefficient was achieved. Yoon et al. [13] also developed a correlation for the boiling heat transfer coefficient for CO₂ (carbon dioxide). Their experimental study was conducted in a stainless-steel tube with an inner diameter of 7.53 mm, which can be categorized as a conventional channel. The authors reported that the heat transfer coefficient of CO₂ (carbon dioxide) could be predicted with a mean deviation of 15.3%. Jige et al. [14] considered each flow pattern and its transitions in the prediction of the heat transfer coefficient, achieving a mean deviation of 10.7%. Of the existing flow pattern models, each model has its own strength represented by the flow pattern regime analysis, which can only be achieved with experimental measurements. Therefore, a correlation was introduced as an alternative method or as an assessment method for the prediction of heat transfer coefficients.

However, the prediction accuracy can be improved by modifying the existing correlation to fit the heat transfer coefficient of R32 inside a multiport mini-channel tube. In addition, a computational method such as machine learning can be applied as an alternative method to improve the prediction accuracy.

Machine learning for the prediction of the boiling heat transfer coefficient

An alternative method such as a computational method, particularly machine learning, can be used to predict the boiling heat transfer coefficient. Machine learning algorithms work by searching through a set of possible prediction models for the model that best captures the relationship between the descriptive features and the target in a dataset [15]. An artificial neural network, as a subset of machine learning algorithms, is applied in this study.

The operation of a neural network originates from its neurons that carry information-processing units [16]. The structure of an artificial neural network consists of an input layer (x_1, x_2, \dots, x_n), hidden layer, and output layer (y), which have interconnections in between. To make an artificial neural network understand the prediction object, the weighted ($w_1,$

w_2, \dots, w_n) sum of neurons and bias that carry the information of inputs pass through an activation function to produce the output (Eq. 1). A hidden layer is added to the ANN model to process only the neurons that have internal connections to the neural network [16]. The illustration of an artificial neural network is presented in Fig. 1.

$$y = \sum_{i=1}^n w_i x_i \quad (1)$$

The application of neural networks to the prediction of heat transfer was first proposed in 1991 by Thibault and Grandjean [17]. They reported that a neural network can be used to reduce the work required to find a suitable model that fits the experimental data or to find an applicable regression model. Since then, studies on ANN models for predicting the heat transfer coefficient have improved [18–22]. Qiu et al. [18] predicted the boiling heat transfer coefficient using a machine learning method with 16,953 data points with a mean deviation of 14.3%. Hughes et al. [19] and Zhou et al. [20] predicted the condensation heat transfer coefficient by applying an ANN prediction model with mean deviations of 14.1% and 6.8%, respectively.

Although Hughes et al. [18] reported that the RFR (Random Forest Regression) model performed better than other models in the prediction of the condensation heat transfer coefficient, the ANN model is still reliable in providing accurate predictions and can be a promising approach in the prediction of heat transfer coefficients. In fact, there are studies reporting the use of ANN models that provided good prediction performance even with a small dataset. Zhu et al.

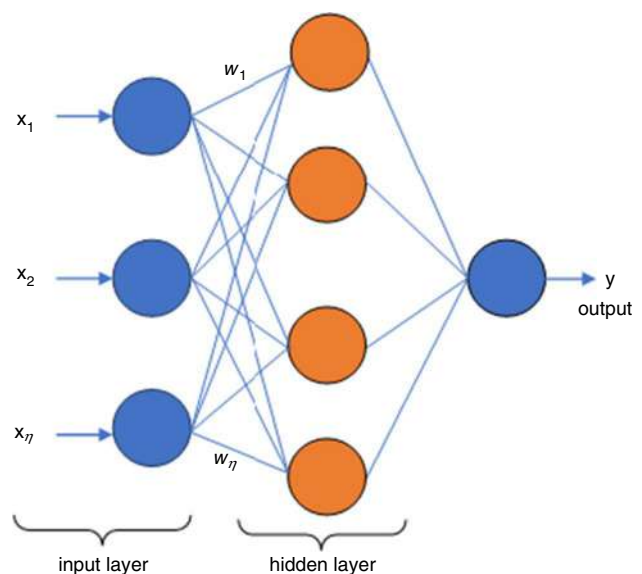


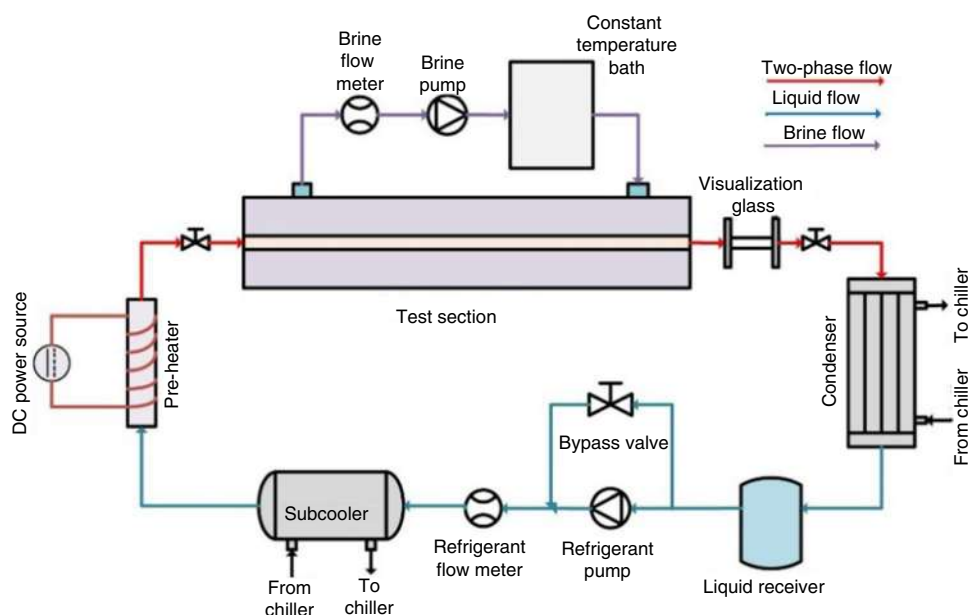
Fig. 1 Structure of an artificial neural network (ANN)

[21] and Kuang et al. [22] demonstrated that machine learning was a good method for predicting the boiling heat transfer coefficient using databases with under 1,000 data points and produced results with mean deviations of 11.41% and 4.54%, respectively.

The purpose of a neural network is to obtain a model that performs well on predicted data. Usually, even small models are guaranteed to be able to fit a sufficiently small dataset [23]. Comprehensively, a dimensionless number as a factor for enhancing the heat transfer coefficient is used as an input parameter. The selected hidden layer and parameter settings should be considered, and training and testing should be conducted to ensure that the selected parameter settings fit the data.

The application of machine learning to the prediction of heat transfer coefficients, especially for flow boiling heat transfer, requires further study because the available literature is limited. Therefore, the objective of this study is to develop an ANN model to predict the boiling heat transfer coefficient of R32 inside a horizontal multiport mini-channel tube. An experimental study was conducted to analyze the effects of the mass flux, heat flux, and vapor quality on the boiling heat transfer coefficient. The experimental data were compared with three types of correlation models to predict the boiling heat transfer coefficient. A new correlation for the boiling heat transfer coefficient is proposed to correct the accuracy of the correlation models. An improvement in prediction accuracy was achieved by applying an ANN model to the prediction of the boiling heat transfer coefficient with the combination of input parameters. Therefore, ANN studies on heat transfer coefficients were conducted to analyze the prediction accuracy achieved using the ANN model.

Fig. 2 Schematic of the experimental apparatus



Experimental setup

Experimental apparatus

To gather boiling heat transfer coefficient data, an experimental study was conducted inside a horizontal multiport mini-channel tube. A schematic of the experimental apparatus and test section is shown in Figs. 2 and 3, respectively. As shown in Fig. 2, the experimental apparatus comprised two main loops: a refrigerant loop and a water loop [24–26]. A refrigerant is supplied to the test section by controlling the refrigerant pump. The refrigerant passes through the Coriolis mass flow meter where the mass flux is varied from 50–500 kg m⁻² s⁻¹ by controlling the pump speed. Subsequently, the refrigerant enters the subcooler where the heat is rejected. The power supply in the preheater is used to adjust the vapor quality at the inlet of the test section. The vapor phase in the outlet of the test section is condensed in

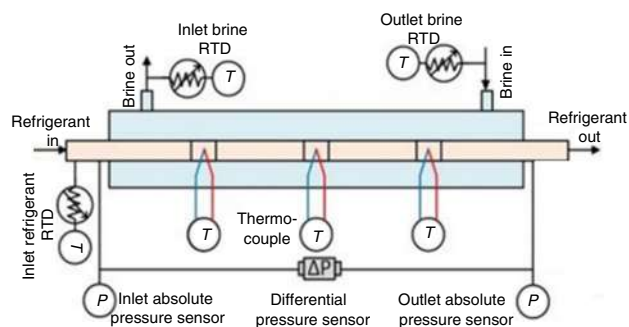


Fig. 3 Schematic of the test section

the condenser and then gathered at the liquid receiver for use in the next cycle.

The temperature is maintained similarly to how the stability of the systems is maintained. The testing system's stability is achieved through heat balancing across the entire testing system. This implies that the applied heat at the test section, heating power at the pre-heater, and heat infiltration from the outer environment must equal the refrigeration effect at the condenser and subcooler. To achieve this, all of the components are controlled together. The heat flux was controlled by controlling the temperature of the bath, and the preheater section heating power was set using the pre-testing calculation with continuous adjustments during operation. The cooling load was controlled by controlling the set temperature of the brine from the separated chiller systems. The control was activated until a relative stability was achieved, implying that the temperature and pressure displayed on the monitor showed only slight fluctuations.

The test section is shown in detail in Fig. 3. The test section is an aluminum multiport mini-channel tube with a hydraulic diameter of 0.969 mm, length of 0.2 m, an aspect ratio of 0.6, and nine channels. Twelve thermocouples were installed on both sides of the wall tube to measure the wall temperature and calculate the heat transfer coefficient.

The location of the thermocouples was distributed at a distance of 50 mm along the test section with two thermocouples attached to each side of every point. All of thermocouples were calibrated to obtain an uncertainty under 0.1 K before being mounted. After mounting, the thermocouples were not removed during the testing of one tube on purpose to maintain the effectiveness of the experiment.

Data reduction and uncertainty

In the experiment, the physical properties of the refrigerants were determined using REFPROP 8. The experimental uncertainties were determined according to ISO guidelines (1995) and are presented in Table 1. Data acquisition by an MX100 Yokogawa was used to convert the experimental results into data.

Table 1 Summary of the parameter uncertainties

Parameter	Uncertainty
$T_{w,in}$	± 0.15
x	$\pm 5\%$
h	$\pm 10\%$
q	$\pm 3\%$
Tube wall thickness/mm	± 0.15
Tube inner diameter/mm	± 0.287

The heat loss was approximately 3%, which was considered in the calibration process. When the calculation of the heat flux was conducted from the heat transfer rate of the test section, which was defined as the mass flow rate and temperature difference between the inlet and outlet of the test section (Eq. 2), the average value of the heat flux was determined by dividing the heat flow rate against the external area of the tube:

$$q = \frac{mc_p(T_{inlet} - T_{outlet})}{A_{external}} \quad (2)$$

To calculate the heat transfer coefficient, the difference between the saturated temperature (T_{sat}) and the inlet wall temperature ($T_{w,in}$) was considered. The inlet wall temperature of the tube was calculated as

$$T_{wall,in} = T_{w,out} + \frac{q\delta}{k} \quad (3)$$

Finally, the heat transfer coefficient was determined using

$$h = \frac{q}{T_{w,in} - T_{sat}} \quad (4)$$

The vapor quality (x) distribution along the test section was then calculated using the enthalpy ratio divided by the latent heat (i_{fg}) in the test section, as per Eq. (5):

$$x = \frac{i - i_f}{i_{fg}} \quad (5)$$

In addition, the inlet quality (x_{in}) and outlet quality (x_{out}) of the test section were determined by Eqs. (6) and (7), respectively:

$$x_{in} = \frac{1}{h_{hf}} \left[\frac{Q}{m_{ref}} - C_{p,ref}(T_{sat} - T_{preheater}) \right] \quad (6)$$

$$x_{out} = x_{in} + m_w C_{p,w}(T_{w,in} - T_{w,out}) \quad (7)$$

According to the ISO guidelines [27], the uncertainties are expressed as listed in Table 1. There were two types of evaluation standard uncertainties that covered the modeling of the measurements. Type A is an evaluation method of uncertainty that is analyzed statistically and is given by the following equation:

$$u^2(x_i) = s^2(\bar{X}_i) = \frac{s^2(X_k)}{n} \quad (8)$$

For an input quantity X_i determined from n independent repeated observations $X_{i,k}$, the standard uncertainty $u(x_i)$ is taken from the estimated $s(\bar{X}_i)$, which is calculated based on Eq. (8), where n is the number of observations.

Type B is used to estimate the input that has not been obtained from repeated observations and is evaluated by scientific judgment based on the available information. Available information may include previous measurement data, manufacturer specifications, or calibration data. The uncertainties in the vapor quality, heat flux, and heat transfer coefficient are determined by modeling the measured parameters that cannot be measured directly. Then, the uncertainties in the vapor quality, heat flux, and heat transfer coefficient can be determined through the functional relationship f (Eq. 9). A summary of the uncertainties is presented in Table 1.

$$Y = f(x_1, x_2, \dots, x_N) \quad (9)$$

Therefore, the accuracy of the thermocouples was tested without applying a heat flux to the test section. Because the acrylic cover of the test section and the space between the tube and the outer environment act as insulation, the thermocouples mounted at the same point showed a similar value under the same conditions, suggesting that the accuracy of the thermocouple was reliable. This test was performed daily. The saturated temperature of the refrigerant was measured at the inlet of the test section using a resistance temperature detector (RTD). An RTD was installed on the water section (inlet and outlet) to measure the water temperature used for heating the test section. Absolute pressure sensors were installed at the inlet and outlet of the test section to measure the saturation pressure. A differential pressure sensor was installed to measure the pressure drop. The recording of experimental data by the MX100 data acquisition

system began when the system maintained the desired mass flux and heat flux for approximately two hours.

Results and discussion

After conducting the experimental study, the effects of the mass flux, heat flux, and vapor quality on the heat transfer coefficient were analyzed. The experimental data were then compared with the superposition, asymptotic, and flow pattern models. This analysis was used to prove the results of the experimental study.

Effect of mass flux and heat flux on heat transfer coefficient

The contribution of convective boiling to the heat transfer coefficient can be monitored by analyzing the effect of the mass flux. Convective boiling was prominent at a higher mass flux, and with an increase in the vapor quality, the heat transfer coefficient was enhanced. When the flow pattern at the high mass flux and in the high vapor quality region exhibited annular flow, the heat transfer coefficient began to decrease owing to the occurrence of dryout. According to Zhu et al. [28], when dryout occurs, the heat transfer coefficient decreases due to the change in the contact area of the vapor at the inner surface of the tube. Therefore, the beginning of dryout was monitored when the heat transfer coefficient decreased at a vapor quality of 0.7. A graph of the heat transfer coefficient versus the vapor quality under various mass flux and fixed heat flux conditions is shown in Fig. 4. The contribution of nucleate boiling to the heat transfer

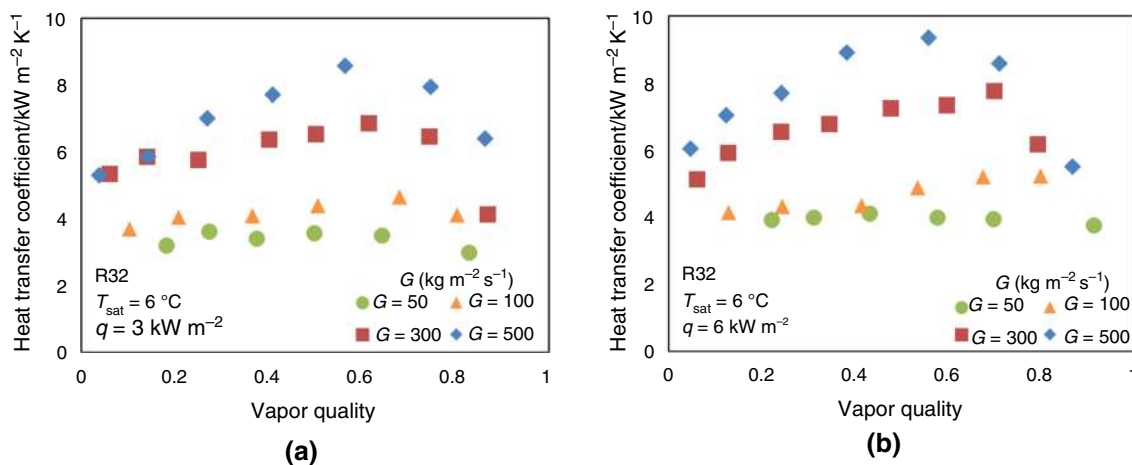


Fig. 4 Effect of mass flux on the heat transfer coefficient of R32 at **a** heat flux of 3 kW m^{-2} and **b** heat flux of 6 kW m^{-2}

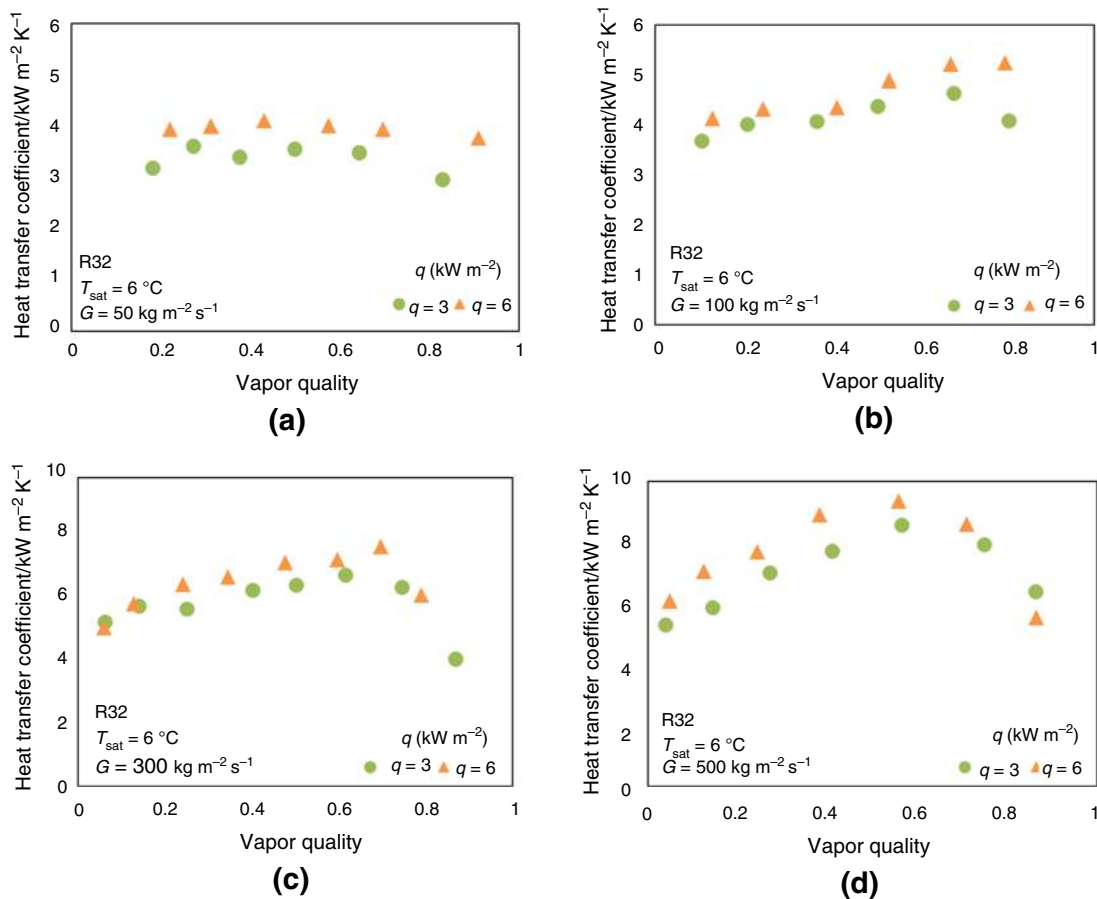


Fig. 5 Effect of heat flux on the heat transfer coefficient at a: **a** mass flux of $50 \text{ kg m}^{-2} \text{ s}^{-1}$, **b** mass flux of $100 \text{ kg m}^{-2} \text{ s}^{-1}$, **c** mass flux of $300 \text{ kg m}^{-2} \text{ s}^{-1}$, and **d** mass flux of $500 \text{ kg m}^{-2} \text{ s}^{-1}$

coefficient can be observed by increasing the heat flux, as shown in Fig. 5. According to Cooper’s pool boiling correlation, which includes the emphatic heat flux, the heat transfer coefficient increased owing to the activation of nucleation, which accelerated the growth of bubbles. According to He et al. [29], due to the strong effect of vapor quality on the mechanisms of heat transfer, convective boiling, and nucleate boiling, the dominance of convective boiling was more pronounced in low superheat conditions rather than nucleate boiling conditions in the low heat flux region, and especially in the low vapor quality region. Therefore, at a low heat flux, the heat transfer coefficients were relatively similar because the effect of nucleate boiling was less or not fully developed when the mass flux was low. As reported by Jige et al. [30], the dryout conditions affected the decrease in the heat transfer coefficient when the vapor quality was increased in the multiport mini-channel tube. Similar to the effect of mass flux on the heat transfer coefficient, the occurrence of dryout was monitored at a high vapor quality of approximately 0.7.

$$\text{Mean deviation} = \frac{1}{n} \sum_{i=0}^n \left| \frac{h_{\text{tp_pred}} - h_{\text{tp_exp}}}{h_{\text{tp_exp}}} \right| \times 100\% \quad (10)$$

$$\text{Average deviation} = \frac{1}{n} \sum_{i=0}^n \left(\frac{h_{\text{tp_pred}} - h_{\text{tp_exp}}}{h_{\text{tp_exp}}} \right) \times 100\% \quad (11)$$

$$R^2 = 1 - \frac{\sum_{i=1}^n (h_{\text{tp_exp}} - h_{\text{tp_pred}})^2}{\sum_{i=1}^n (h_{\text{tp_exp}} - \bar{h}_{\text{tp}})^2} \quad (12)$$

where $\bar{h}_{\text{tp}} = \frac{1}{n} \sum_{i=1}^n h_{\text{tp_exp}}$.

Assessment of the boiling heat transfer coefficient

The experimental data were compared with the superposition model [2–5], asymptotic model [7–10], and flow pattern model [11–14]. The assessment of the existing correlations

Table 2 Error analysis of the compared correlations

Correlation	Error analysis		
	Mean deviation/%	Average deviation/%	R^2
Gungor and Winterton (1986)	73.53	- 73.53	0.38
Jung et al. (1989)	64.87	- 64.87	0.06
Li et al. (2013)	74.08	- 74.08	0.53
Mahmoud and Karayiannis (2013)	80.04	- 80.04	0.07
Liu and Winterton (1991)	36.01	- 18.50	0.72
Steiner and Taborek (1992)	45.85	18.57	0.65
Wattelet et al. (1994)	40.63	- 2.57	0.66
Tapia and Ribatski (2017)	66.32	- 65.63	0.48
Kattan–Thome–Favrat (1998)	57.76	- 55.82	0.01
Thome and El Hajal (2004)	38.97	7.69	0.47
Yoon et al. (2004)	42.10	- 17.39	0.39
Jige et al. (2019)	81.69	- 81.69	0.72

compared with the experimental data in this study was conducted through an error analysis expressed as Eqs. (10) and (11). In addition, the coefficient of determination (R^2) was calculated using Eq. (12) to determine the reliability of the fitting indicator to the models.

A summary of the existing boiling correlations is presented in Appendix A, and the error analysis for each model against the experimental data is presented in Table 2. Figure 6 shows a comparison of the empirical correlation with the experimental data for R32 inside a horizontal multiport mini-channel tube.

A best fit empirical correlation for the prediction of the heat transfer coefficient can be observed from the data trend in Fig. 6. Moreover, the error analysis helped to indicate which empirical correlation predicted the heat transfer coefficient of R32 inside a multiport mini-channel tube with a small error percentage. Therefore, from Table 2 and Fig. 6, it can be observed that the correlation by Liu and Winterton

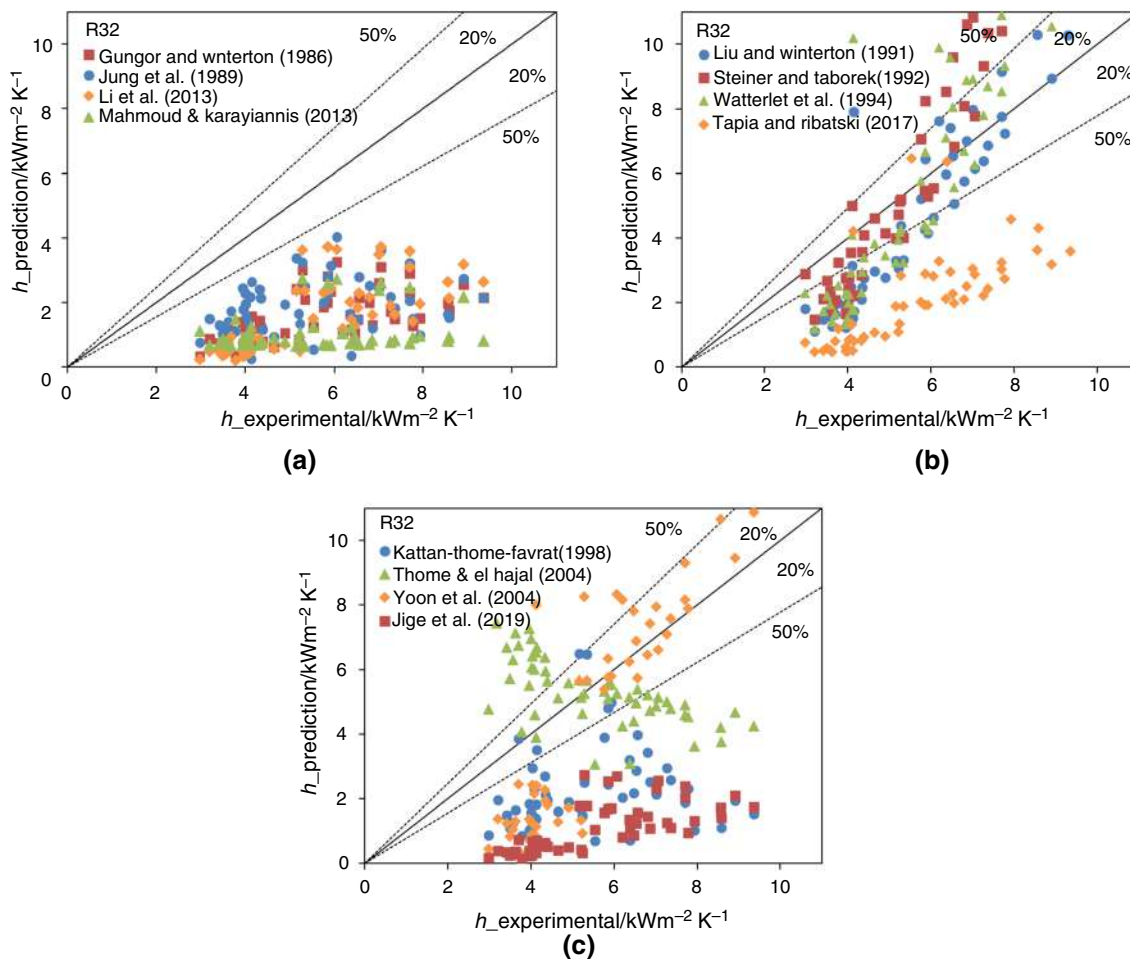


Fig. 6 Comparison of the heat transfer coefficient correlation of R32 with the **a** superposition model, **b** asymptotic model, and **c** flow pattern model

[7] accomplishes the best fit prediction of the heat transfer coefficient of R32 inside a multiport mini-channel tube with a mean deviation of 36.01%. However, an overall analysis shows that the comparison of the superposition, asymptotic, and flow pattern models is limited to the prediction of the heat transfer coefficient of R32 inside a multiport mini-channel tube. This may be due to the differences in the amount of data, channel geometry, or refrigerants that were applied while developing the correlation. Therefore, an empirical correlation for R32 inside a multiport mini-channel tube was developed by modifying the convective boiling term by Bertsch et al. [31] with the sum of the liquid and vapor phase Dittus–Boelter correlations and applying a two-phase Nusselt number with the correction factors Bd , Fr_{10} , We_v , and Bo . The new empirical correlation is as follows:

$$h_{cb} = [h_l(1 - x) + h_v x] \tag{13}$$

$$h_l = 0.023 \frac{k_l}{D} Re_{10}^{0.8} Pr_1^{0.4} \tag{14}$$

$$h_v = 0.023 \frac{k_l}{D} Re_{v0}^{0.8} Pr_v^{0.4} \tag{15}$$

$$Nu_{tp} = Bd^{-2.329} Bo^{0.2} Fr_{10}^{0.7} We_v^{0.1354} h_{cb}^{1.342} \tag{16}$$

This new empirical correlation produced a mean deviation of 10.33% and an average deviation of 4.64% against the experimental data, demonstrating that this correlation improved the prediction accuracy for the boiling heat transfer coefficient of R32 inside a multiport mini-channel tube.

Proposed ANN model

The high uncertainty of the prediction when applying an empirical correlation to the heat transfer coefficient is the main reason to build a new data-based configuration. An ANN model offers an improvement in prediction accuracy to the boiling heat transfer coefficient of R32 inside a multiport mini-channel tube.

ANN model parameter

As mentioned in Fig. 1, the structure of the ANN model in this study consists of an input layer, hidden layer, and output layer; thus, this type of network is also called a multilayer perceptron neural network. A multilayer perceptron (MLP) connects the neurons in one layer to the previous layer through masses [16]. Before an ANN produces an output through the input data, the ANN model must learn how to read the pattern of data. To make the ANN model achieve a good prediction of the heat transfer coefficient, the model

Table 3 ANN model setting parameters

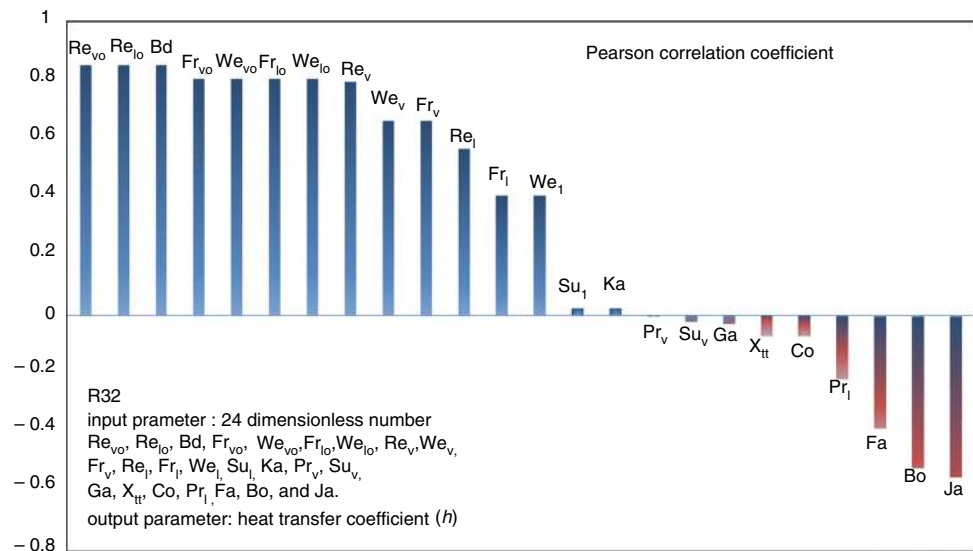
Parameter	Value
Activation function	ReLU
Optimizer	Adam
Split function	Repeated <i>k</i> -fold cross-validation
Loss function	Mean absolute error
Batch size	20
Epoch	1500
Learning rate	0.001
Exponential decay rate for estimates of first-moment vector, β_1	0.9
Exponential decay rate for estimates of second-moment vector, β_2	0.999
Dropout	0.5

should be trained with a modification of the setting parameters based on the structure of the data (Table 3).

The experimental data were modified for use as prediction data. A total of 467 data points were collected from the modified calculation of the raw experimental data, which were divided into training data (70%), validation data (10%), and testing data (20%) by applying a repeated *k*-fold cross-validation. Repeated *k*-fold cross-validation with fivefold or splits is used to divide data into different repetitions. The Panda, Keras, and Scikit-Learn libraries were used to create the model in Python. The pre-processing data were obtained with a min–max scaler function with a range of – 1 to 1 before applying the hidden layer and activation function. The ANN model setting parameters used in this study are listed in Table 3.

A rectified linear unit (ReLU) is a nonlinear activation function that is usually used for deep learning neural networks owing to its capability to produce a strong gradient to achieve better performance. Adam, an algorithm for first-order gradient-based optimization of stochastic objective functions that is based on adaptive estimates of lower-order moments, was selected as the optimization function [32]. A gradient-based optimization could also be used to change the output error due to the changes in the masses to minimize the error [16]. Moreover, Adam works as an optimizer by updating the masses in the training data, which can affect the decision of the output value. The masses of each neuron carry the information to be multiplied by the input and bias. To update the masses, a mean absolute error is selected as the loss function, where the difference between the input and predicted value is considered to minimize the loss on the next prediction. In addition, to further minimize the loss,

Fig. 7 Pearson correlation coefficient of input parameters in relation to the heat transfer coefficient



the batch size was set to 20, implying that the ANN model trained and tested the data with 19 iterations. An increase in the number of epochs can also reduce model loss, considering more masses changes. The learning rate was set to 0.001 to obtain an optimum step size that could update the masses for the next iteration. The batch, epochs, and learning rate also affected the training time of the ANN model, which underwent the forward and backward propagation. Finally, to avoid overfitting the prediction, the dropout/tolerance was set to 0.5.

Because the ANN model was set with the previously mentioned parameters, the input parameters were determined using the Pearson correlation coefficient based on the analysis method by Zhou et al. [20]. The Pearson correlation coefficient was positive, indicating that if the input parameter increased, the output parameter of the heat transfer coefficient also increased, whereas if the value was negative, the heat transfer coefficient decreased if the input parameter increased [33]. Based on the Pearson correlation coefficients (Fig. 7), the 24 dimensionless parameters can be arranged as follows from the highest positive rank to the highest negative

Table 4 Parameter settings of other ANN models

Parameter	Value		
	Qiu et al. [18]	Hughes et al. [19]	Zhou et al. [20]
Hidden layer	(75,70,60,50,30,20,10)	(20,16,14,10)	(150,140,130,120,110,100,90,80,70,60,50,40,30,20,10)
Activation function	ReLU	ReLU	ReLU
Optimizer	Adam	Adam	Adam
Batch size	200	200	200
Epoch	1500	1500	1500
Learning rate	0.001	0.001	0.001
Exponential decay rate for estimates of first-moment vector, β_1	0.9	0.9	0.9
Exponential decay rate for estimates of second-moment vector, β_2	0.999	0.999	0.999
Dropout/tolerance	0.001	0.001	0.001
Input parameter	Co, Bd, Bo, Fr _l , Fr _{lo} , Fr _v , Fr _{vo} , Pr _l , Pr _v , Re _l , Re _{lo} , Re _v , Re _{vo} , Su _l , Su _v , We _l , We _{lo} , We _v , We _{vo}	x, Re _v , Re _l , Fr _v , Fr _l , Bo, We, aspect ratio, Pr _v , Pr _l , Ja	Bd, Co, Fr _l , Fr _{lo} , Fr _v , Fr _{vo} , Ga, Ka, Pr _v , Pr _l , Re _l , Re _{lo} , Re _v , Re _{vo} , Su _l , Su _v , Su _{vo} , Su _{vo} , We _l , We _{lo} , We _v , We _{vo}

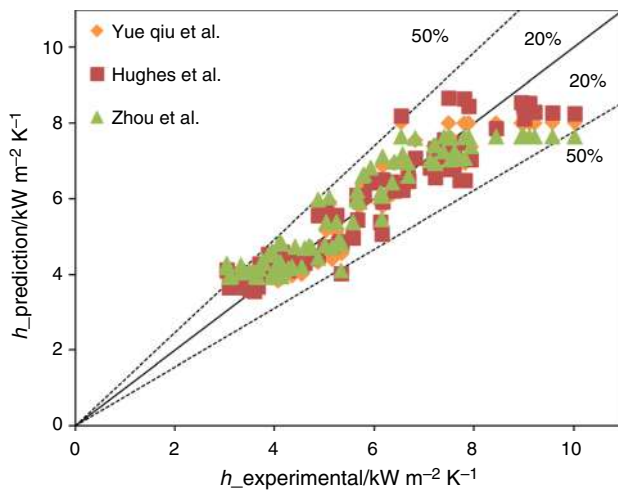


Fig. 8 Comparison of the ANN predictions with those of other ANN models proposed by Qiu et al. [18], Hughes et al. [19], and Zhou et al. [20]

rank: Re_{vo} , Re_{lo} , Bd , Fr_{vo} , We_{vo} , Fr_{lo} , We_{lo} , Re_v , We_v , Fr_v , Re_l , Fr_l , We_l , Su_l , Ka , Pr_v , Su_v , Ga , X_{tt} , Co , Pr_l , Fa , Bo , and Ja . In addition, the heat transfer coefficient was set to be an output parameter.

Assessment of the ANN model parameters

To evaluate whether the chosen parameter settings could be applied well to the proposed ANN model, the parameter settings proposed by Qiu et al. [18], Hughes et al. [19], and Zhou et al. [20] were used to train and test the ANN models

using the experimental data of R32 inside a multiport mini-channel tube (Table 4). The models with the parameter settings used by Qiu et al. [18], Hughes et al. [19], and Zhou et al. [20] exhibited similar patterns with mean deviations of 9.15%, 8.29%, and 9.89%, respectively. Although the models with the settings used by Hughes et al. [19] and Zhou et al. [20] were used to predict the condensation heat transfer coefficient, they provided accurate predictions of the boiling heat transfer coefficient of R32 inside a multiport mini-channel tube, as shown in Fig. 8.

Regardless of the good result on this assessment of ANN model parameters, the ANN model setting parameters in Table 4 were not represented the actual model due to ANN’s characteristic as a “black box” model as mentioned by Prieto et al. [34] in their previous study. In addition, Thibault and Grandjean [17] reported that the purpose of neural networks is to simplify the determination of an appropriate model to fit experimental data to the heat transfer coefficient. Therefore, beside the insufficiency of ANN model on showing its true value inside the hidden layer or the prediction model, ANN model was able to improve the prediction accuracy by modifying an existed setting parameters to a new model.

ANN model prediction

The input parameters selected using the Pearson correlation coefficient were used to train and test the ANN model. The performances of the ANN models with the same hidden layer of (96,72,48,24), but different numbers of input parameters were compared (Table 5). The test began with 24 input parameters; then, two parameters were eliminated for the

Table 5 ANN model selection of R32 with different numbers of input parameters

Test number	Hidden layer	Input parameter	Average deviation/%	Mean deviation/%	R^2
1	(96,72,48,24)	24 inputs: Re_{vo} , Re_{lo} , Bd , Fr_{vo} , We_{vo} , Fr_{lo} , We_{lo} , Re_v , We_v , Fr_v , Re_l , Fr_l , We_l , Su_l , Ka , Pr_v , Su_v , Ga , X_{tt} , Co , Pr_l , Fa , Bo , and Ja	- 3.04	9.24	0.90
2		22 inputs: Re_{vo} , Re_{lo} , Bd , Fr_{vo} , We_{vo} , Fr_{lo} , We_{lo} , Re_v , We_v , Fr_v , Re_l , Fr_l , We_l , Su_l , Pr_v , Su_v , Ga , X_{tt} , Co , Pr_l , Fa , Bo	- 1.17	8.22	0.85
3		20 inputs: Re_{vo} , Re_{lo} , Bd , Fr_{vo} , We_{vo} , Fr_{lo} , We_{lo} , Re_v , We_v , Fr_v , Re_l , Fr_l , We_l , Pr_v , Su_v , Ga , X_{tt} , Co , Pr_l , and Bo	0.00	8.46	0.86
4		18 inputs: Re_{vo} , Re_{lo} , Bd , Fr_{vo} , We_{vo} , Fr_{lo} , We_{lo} , Re_v , Fr_v , Re_l , Fr_l , We_l , Pr_v , Su_v , X_{tt} , Co , Pr_l , and Bo	- 0.72	9.97	0.81
5		16 inputs: Re_{vo}, Re_{lo}, Bd, Fr_{vo}, We_{vo}, Fr_{lo}, We_{lo}, Re_v, Fr_v, Re_l, We_l, Pr_v, X_{tt}, Co, Pr_l, Bo*	1.35	6.35	0.91
6		14 inputs: Re_{vo} , Re_{lo} , Bd , Fr_{vo} , We_{vo} , Fr_{lo} , We_{lo} , Re_v , We_v , Fr_v , Re_l , We_l , Pr_l , Bo	0.54	8.14	0.84
7		12 inputs: Re_{vo} , Re_{lo} , Bd , Fr_{vo} , We_{vo} , Fr_{lo} , We_{lo} , Re_v , We_v , Fr_v , Pr_l , Bo	4.27	9.90	0.84
8		10 inputs: Re_{vo} , Re_{lo} , Bd , Fr_{vo} , We_{vo} , Fr_{lo} , We_{lo} , Re_v , Pr_l , Bo	4.20	8.35	0.90
9		8 inputs: Re_{vo} , Re_{lo} , Bd , Fr_{vo} , We_{vo} , Fr_{lo} , Pr_l , and Bo	- 1.9	12.0	0.79
10		6 inputs: Re_{vo} , Re_{lo} , Bd , We_{vo} , Pr_l , and Bo	- 1.89	11.03	0.75

*Final selected input parameter

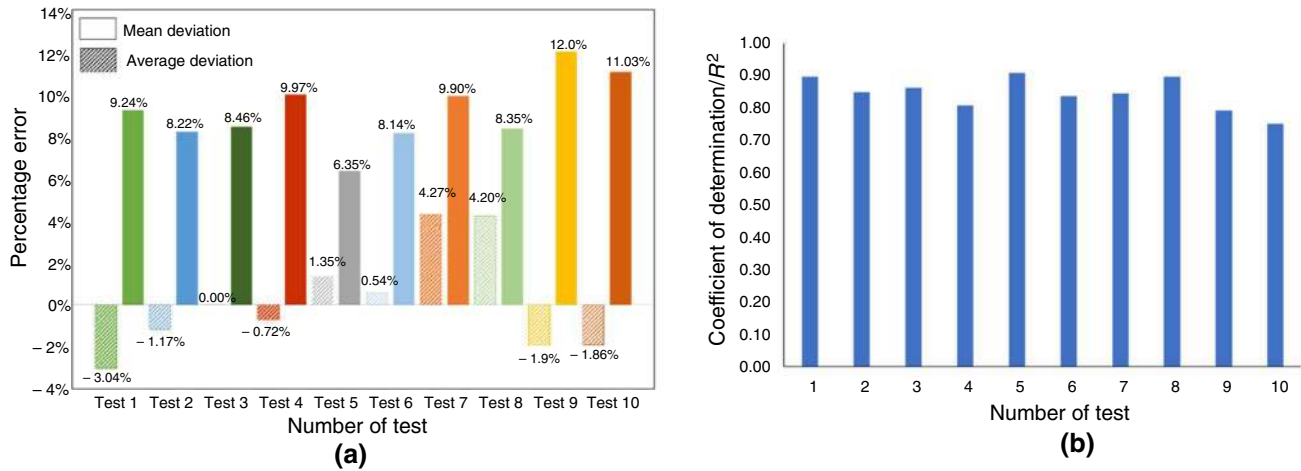


Fig. 9 Error analysis of ANN model selection for R32 with different input parameters **a** MD and AD, and **b** R²

next cases. There were 10 cases in total that were randomly arranged based on the positive rank and negative rank of the Pearson correlation coefficient. .

The best fit prediction result was achieved with an ANN model with 16 input parameters, of which the mean deviation was lower than that using the other combinations of input parameters as shown in Fig. 9. Figure 9a presents the mean deviation and average deviation of the prediction results, where the lowest mean deviation (MD) was taken as the best fit ANN model in the prediction of the heat transfer coefficient of R32 inside a multiport mini-channel tube; Fig. 9b shows the coefficient of determination for each test.

Then, the chosen input parameters, or more specifically, 16 dimensionless numbers were evaluated through 10 prediction cases with different hidden layers (Table 6).

The results show that the ANN model with 4 hidden layers (96,72,48,24) demonstrated the lowest mean deviation and highest coefficient of determination, indicating that the prediction was well aligned with the experimental data as presented in Fig. 10. Figure 11 shows the number of epochs used to reduce the model loss. One epoch implies that the dataset was passed forward and backward through the neural network. As previously mentioned, to complete the process of 1 epoch, the ANN model proceeds through 19 iterations. Figure 12 shows a comparison of the experimental data versus the predictions of the heat transfer coefficient obtained with the ANN using the selected hidden layer and input parameters. The predicted heat transfer coefficient tends to be along the middle line, indicating good accuracy.

Table 6 ANN model selection for R32 with different hidden layers

Number of tests	Input parameters	Hidden layer	Average deviation/%	Mean deviation/%	R ²
1	16 inputs: Re _{vo} , Re _{lo} , Bd, Fr _{vo} , We _{vo} , Fr _{lo} , We _{lo} , Re _v , Fr _v , Re _l , We _l , Pr _v , X _{tt} , Co, Pr _l , and Bo	100 90 80 70 60 50 40 30 20 10	- 6.06	12.34	0.86
2		100 90 80 70 60 50 40 30 20	- 9.08	13.67	0.86
3		100 90 80 70 60 50 40 30	18.40	23.71	0.64
4		100 90 80 70 60 50 40	- 9.10	13.05	0.87
5		100 90 80 70 60 50	- 8.23	10.96	0.84
6		100 90 80 70 60	- 6.36	10.32	0.87
7		100 90 80 70	- 4.88	9.55	0.83
8		120 96 72 48 24	0.75	8.71	0.89
9		120 96 72 48	1.35	10.02	0.88
10		96 72 48 24*	1.35	6.35	0.91

*Final selected hidden layer

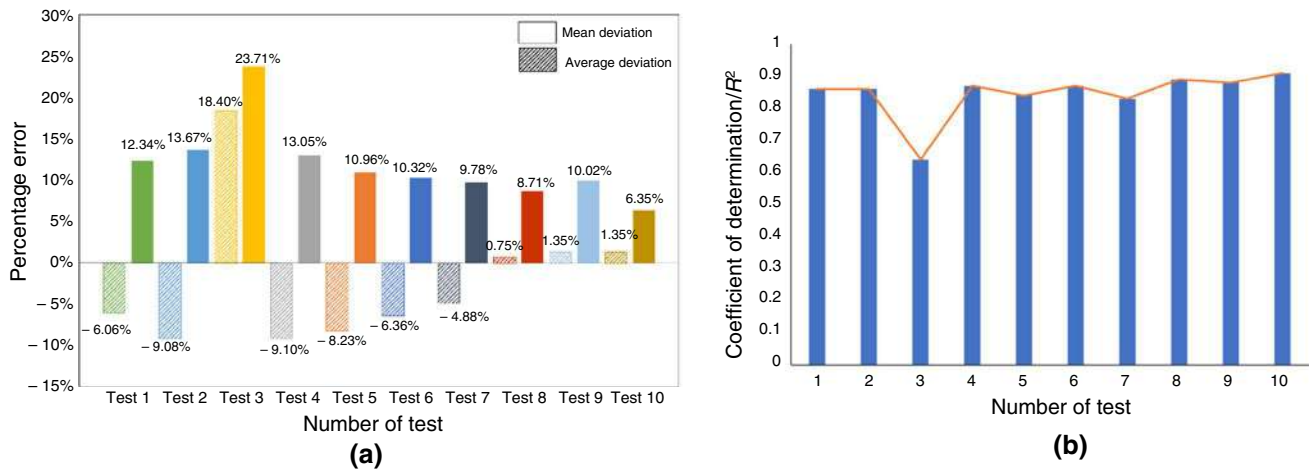


Fig. 10 Error analysis of the ANN model selection for R32 with different hidden layers: a MD and AD, and b R^2

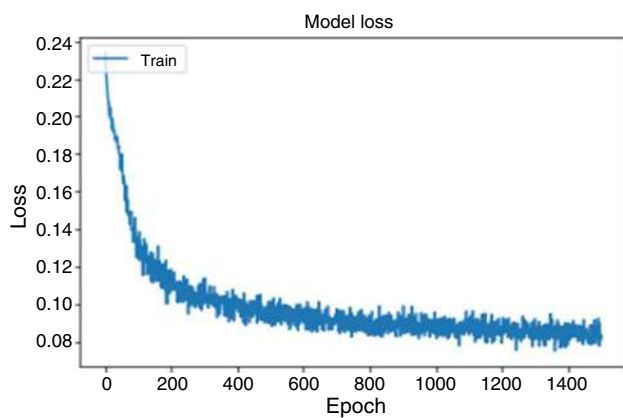


Fig. 11 ANN model loss

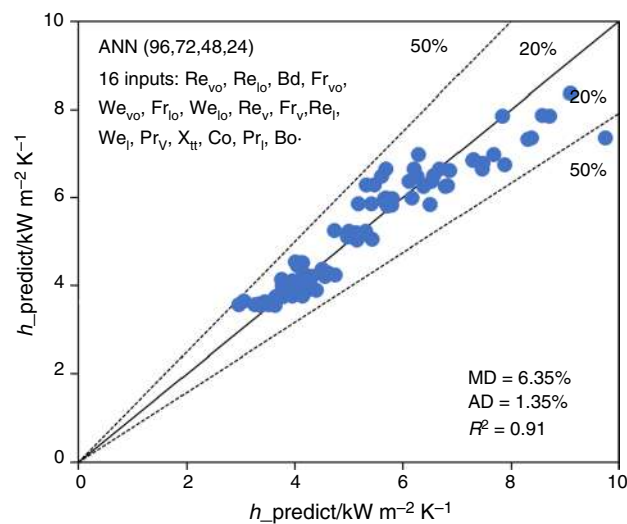


Fig. 12 Comparison of the ANN predictions and experimental data

This high accuracy in the prediction of the boiling heat transfer coefficient of R32 compared with the superposition model, asymptotic model, and flow pattern model is a result of the proposed prediction model achieved by the ANN due to the model’s capability of recognizing data trends.

Conclusions

An experimental study of the boiling heat transfer coefficient of R32 inside a horizontal multiport mini-channel tube with a hydraulic diameter of 0.969 mm, nine channels, and an aspect ratio of 0.6 was conducted. The heat transfer coefficient increased with increasing mass and heat flux. Dryout occurred at an approximate vapor quality of 0.7. The experimental data were divided into training data (70%), validation data (10%), and testing data (20%) and used by a machine learning algorithm to predict the boiling heat transfer coefficient. There were 16 input parameters, consisting of dimensionless numbers. The ANN model with 4 hidden layers of (96,72,48,24) achieved a good prediction of the boiling heat transfer coefficient of R32 inside a multiport mini-channel tube with a mean deviation of 6.35%. A comparison of the experimental data with the existing correlations from the superposition model, asymptotic model, and flow pattern model and the proposed correlation resulted in a higher mean deviation compared with the ANN prediction model. Although each model has its advantages, the ANN model, as a data-based model method, can serve as an alternative method to improve the prediction of the heat transfer coefficient, especially for multiport mini-channel tubes.

Appendix A

Author	Correlation	Details
Gungor and Winterton [2] (1986)	$h_{tp} = Eh_1 + Sh_{pool}$ $h_1 = 0.023Re_L^{0.8}Pr_L^{0.4} \left(\frac{k_l}{d}\right)$ $E = 1 + 24000Bo^{1.16} + 1.37(1/X_{tt})^{0.86}$ $h_{pool} = 55p_r^{0.12}(-\log_{10} p_r)^{-0.55}M^{-0.5}q^{0.67}$ $S = \frac{1}{1+1.15 \times 10^{-6}E^2Re_L^{1.17}}$ <p>For horizontal tube and $Fr < 0.05$:</p> $E = Fr^{(0.1-2Fr)}, S = \sqrt{Fr}$	4300 data points Working fluid: water, R11, R12, R22, R113, R114, Ethylene glycol D_h from 2.95 to 32 mm
Jung et al. [3] (1989)	$h_{tp} = Sh_{nb} + Fh_{lo}$ $h_{nb} = 207Pr_1^{0.533} \left(\frac{k_l}{d}\right) \left(\frac{qD_b}{k_j T_{sat}}\right)^{0.745} \left(\frac{\rho_v}{\rho_l}\right)^{0.581}$ $D_b = 0.51 \left[\frac{2\sigma}{g(\rho_l - \rho_v)}\right]^{0.5}$ $h_{lo} = 0.023Re_L^{0.8}Pr_L^{0.4} \left(\frac{k_l}{d}\right)$ $S = \begin{cases} 4048X_{tt}^{1.22}Bo^{1.13} & \text{if } X_{tt} < 1 \\ 2 - 0.1X_{tt}^{-0.28}Bo^{0.33} & \text{if } 1 < X_{tt} < 5 \end{cases}$ $F = 2.37 \left(0.29 + 1/X_{tt}\right)^{0.85}$	2000 data points Working fluid: R12/R152a mixture, R22/R114 mixture Inner diameter: 9 mm
Mahmoud and Karayiannis [4] (2013)	$h_{tp} = h_{cooper} \cdot S + h_L \cdot F$ $h_{cooper} = 55p_r^{0.12}(-\log_{10} p_r)^{-0.55}M^{-0.5}q^{0.67}$ $h_L = \begin{cases} 4.36 \frac{k_l}{d} & Re_L < 2000 \\ 0.023Re_L^{0.8}Pr_L^{0.4} \left(\frac{k_l}{d}\right) & Re_L > 3000 \end{cases}$ $F = \left(1 + \frac{2.812Co^{-0.408}}{X_{tt}}\right)^{0.64}$ $S = \frac{1}{1+2.56 \times 10^{-6}(Re_L F^{1.25})^{1.17}}$	5152 data points Working fluid: R134a, D_h from 0.52 to 4.26 mm
Li et al. [5] (2013)	$h_{tp} = Sh_{nb} + Fh_{cb}$ $h_{nb} = 55p_r^{0.12}(-\log_{10} p_r)^{-0.55}M^{-0.5}q^{0.67}$ $h_{nb} = 0.023Re_L^{0.8}Pr_L^{0.4} \left(\frac{k_l}{d}\right)$ $F = \frac{1+1.8(0.3+1/X_{tt})^{0.88}}{1+We_v^{-0.4}}$ $S = \frac{1}{0.5+0.5 \frac{(Re_{tp} \times 10^{-3})^{0.3}}{(Bo \times 10^3)^{0.23}}}$ $Re_{tp} = Re_L F^{1.25}$	Working fluid: R1234yf, R32, R32/R1234yf mixture D_h from 2.95 to 32 mm
Liu and Winterton [7] (1991)	$h_{tp}^2 = (Fh_L)^2 + (Sh_{pool})^2$ $F = \left[1 + xPr_1 \left(\frac{\rho_l}{\rho_v} - 1\right)\right]^{0.35}$ $S = (1 + 0.055F^{0.1}Re_1^{0.16})^{-1}$ $h_L = 0.023 \left(\frac{k_l}{d}\right) Re_L^{0.8} Pr_L^{0.4}$ $h_{pool} = 55p_r^{0.12}q^{2/3}(-\log_{10} p_r)^{-0.55}M^{-0.5}$	476 data points Working fluid: R32, R1234yf, mixture refrigerant (R32 and R1234yf) D_h : 2 mm

Author	Correlation	Details
Steiner and Taborek [8] (1992)	$h_{tp} = \left[(h_{nb})^3 + (h_{cb})^3 \right]^{\frac{1}{3}}$ $h_{nb} = 55 p_r^{0.12} (-\log_{10} P_r)^{-0.55} M^{-0.5} q^{0.67}$ $h_{cb} = h_l F_{fp}$ $h_l = 0.023 \frac{k_l}{D} \text{Re}_{lo}^{0.8} \text{Pr}_l^{0.4}$ $\text{Re}_{lo} = \frac{GD}{\mu_l}$ $F_{fp} = \left(\left[(1-x)^{1.5} + 1.9(x)^{0.6}(1-x)^{0.01} \left(\frac{\rho_l}{\rho_v} \right)^{0.35} \right]^{-2.2} + \left[\left(\frac{h_v}{h_l} \right) (x)^{0.01} (1 + 8(1-x)^{0.7}) \left(\frac{\rho_l}{\rho_v} \right)^{0.67} \right]^{-2} \right)^{-0.5}$	13,000 data points Working fluid: inorganic and organic fluids, water, seven hydrocarbons, four refrigerants, He, N ₂ , H-para, and NH ₃
Wattelet et al. [9] (1994)	$h_{tp} = \left[(h_{nb})^{2.5} + (h_{cb})^{2.5} \right]^{\frac{1}{2.5}}$ $h_{nb} = 55 p_r^{0.12} (-\log_{10} P_r)^{-0.55} M^{-0.5} q^{0.67}$ $h_{cb} = F h_l R$ $h_l = 0.023 \frac{k_l}{D} \text{Re}_{lo}^{0.8} \text{Pr}_l^{0.4}$ $F = 1 + 1.925 X_{tt}^{-0.83}$ $X_{tt} = \left(\frac{1-x}{x} \right)^{0.9} 0.551 p_r^{0.492}$ $R = \begin{cases} 1.32 F_l^{0.2} & \text{if } \text{Fr}_l < 0.25 \\ 1 & \text{if } \text{Fr}_l \geq 0.25 \end{cases}$	Working fluid: R12, R134a, and refrigerant mixture Inner diameter of 7.04 mm
Tapia and Ribatski. [10] (2017)	$h_{tp} = \left[(F h_l)^2 + (S h_{nb})^2 \right]^{0.5}$ $F = 1 + \left(\frac{2.55 X_{tx}^{-1.04}}{1 + \text{We}_{uv}^{-0.194}} \right)$ $X_{tx} = \begin{cases} X_{tt} = \left(\frac{1-x}{x} \right)^{0.9} \left(\frac{\rho_v}{\rho_l} \right)^{0.5} \left(\frac{\mu_l}{\mu_v} \right)^{0.1} & \text{for } \text{Re}_v > 1000 \\ X_{tt} = \frac{1}{18.7} \text{Re}_{v,0}^{0.4} \left(\frac{1-x}{x} \right)^{0.9} \left(\frac{\rho_v}{\rho_l} \right)^{0.5} \left(\frac{\mu_l}{\mu_v} \right)^{0.1} & \text{for } \text{Re}_v \leq 1000 \end{cases}$ $\text{We}_{uv} = \frac{\rho_v u_v^2 d}{\sigma}, \quad u_v = \frac{Gx}{\rho_v \alpha}$ $\alpha = \left[1 + 1.021 \text{Fr}_m^{-0.092} \left(\frac{\mu_l}{\mu_v} \right)^{-0.368} \left(\frac{\rho_l}{\rho_v} \right)^{1/3} \left(\frac{1-x}{x} \right)^{2/3} \right]^{-1}$ $S = \frac{1.427 \text{Bd}^{0.032}}{1 + 0.1086 (10^{-4} \text{Re}_{lo} F^{1.25})^{0.981}}$ $h_l = 0.023 \frac{k_l}{D} \text{Re}_{lo}^{0.8} \text{Pr}_l^{0.4}$ $h_{nb} = 207 \text{Pr}_l^{0.533} \left(\frac{k_l}{d} \right) \left(\frac{gd}{k_l T_{sat}} \right)^{0.745} \left(\frac{\rho_v}{\rho_l} \right)^{0.581} \left(\frac{\mu_l \rho_l c_p}{k_l} \right)^{0.533}$	3409 data points Inner diameter: 1.1 mm Working fluid: R134a, R1234ze(E), R1234yf, R600a
Kattan-Thome-Favrat [11] (1998)	$h_{tp} = \frac{\theta_{dry} h_v + (2\pi - \theta_{dry}) h_{wet}}{2\pi}$ $h_{wet} = (h_{cb}^3 + h_{nb}^3)^{1/3}$ $h_v = 0.023 \text{Re}_v^{0.8} \text{Pr}_v^{0.4} \frac{k_v}{D}$ $h_{cb} = 0.0133 \text{Re}_l^{0.69} \text{Pr}_l^{0.4} \frac{k_l}{\delta}$ $h_{nb} = 55 p_r^{0.12} (-\log_{10} P_r)^{-0.55} M^{-0.5} q^{0.67}$ $\theta_{dry} = \theta_{strat} \frac{G_{high} - G}{G_{high} - G_{low}}$ $\theta_{strat} = 2\pi - 2 \left\{ \begin{aligned} & \pi(1-\alpha) + \left(\frac{3\pi}{2} \right)^{\frac{1}{3}} \left[1 - 2(1-\alpha) + (1-\alpha)^{\frac{1}{3}} - \alpha^{\frac{1}{3}} \right] \\ & - \frac{1}{200} (1-\alpha)\alpha [1 - 2(1-\alpha)] \left[1 + 4((1-\alpha)^2 + \alpha^2) \right] \end{aligned} \right\}$	702 data points Working fluid: R134a, R123, R402A, R404A, R502

Author	Correlation	Details
Thome and El Hajal [12] (2004)	$h_{tp} = \frac{\theta_{dry} h_v + (2\pi - \theta_{dry}) h_{wet}}{2\pi}$ $h_{wet} = (h_{cb}^3 + h_{nb}^3)^{1/3}$ $h_v = 0.023 Re_v^{0.8} Pr_v^{0.4} \frac{k_v}{D}$ $h_{cb} = 0.0133 Re_\delta^{0.69} Pr_1^{0.4} \frac{k_1}{\delta}$ $h_{nb} = 55 p_r^{0.12} (-\log_{10} p_r)^{-0.55} M^{-0.5} q^{0.67}$ $Re_\delta = [4G(1-x)\delta] / [\mu_l(1-\epsilon)]$ $\epsilon = \frac{x}{\rho_v} \left\{ [1 + 0.12(1-x)] \left(\frac{x}{\rho_v} + \frac{1-x}{\rho_l} \right) + \frac{1.18(1-x)}{G} \left[\frac{g\sigma(\rho_l - \rho_v)}{\rho_l^2} \right]^{0.25} \right\}^{-1}$ $\delta = [\pi D(1-\epsilon)] / [2(2\pi - \theta_{dry})]$	404 Data points Working fluid: CO ₂ D _h from 0.79 to 10.06 mm
Yoon et al. [13] (2004)	$h_{tp} = [Sh_{nb}^2 + (Eh_l)^2]^{1/2} \quad \text{if } x < x_{crit}$ $h_{nb} = 55 p_r^{0.12} (-\log_{10} p_r)^{-0.55} M^{-0.5} q^{0.67}$ $S = \frac{1}{1 + 1.62 \times 10^{-6} Re_l^{1.11}}$ $E = \left[1 + 9.36 \times 10^3 x Pr_1 + \left(\frac{\rho_l}{\rho_v} - 1 \right) \right]^{0.86}$ $h_l = 0.023 \frac{k_l}{D} Re_{lo}^{0.8} Pr_1^{0.4}$ $h_v = 0.023 Re_v^{0.8} Pr_v^{0.4} \frac{k_v}{D}$ $h_{wet} = 1 + 3000 Bo^{0.86} + 1.12 \left(\frac{x}{1-x} \right)^{0.75} \left(\frac{\rho_l}{\rho_v} \right)^{0.41}$ $h_{tp} = \frac{\theta_{dry} h_v + (2\pi - \theta_{dry}) h_{wet}}{2\pi} \quad \text{if } x \geq x_{crit}$ $\theta_{dry} = 36.23 Re^{3.47} Bo^{4.84} Bd^{-0.27} \left(\frac{1}{X} \right)^{2.6}$	Working fluid: CO ₂ D _h from 7.53 mm
Jige et al. [14] (2019)	$h_{tp} = (h_{cb}^5 + h_{nb}^5)^{1/5}$ $h_{cb} = \max(h_{fc}, h_{lf})$ $h_{nb} = 10 \frac{k_1}{D_b} \left(\frac{q D_b}{k_1 T_s} \right)^C \left(\frac{P_s}{P_{crit}} \right)^{0.1} \left(1 - \frac{T_s}{T_{crit}} \right)^{-1.4} \left(\frac{\mu_l c p_1}{k_1} \right)^{-0.25}$ $D_b = 0.511 \sqrt{\frac{2\sigma}{g(\rho_l - \rho_v)}}, \quad C = 0.855 \left(\frac{\rho_v}{\rho_l} \right)^{0.309} \left(\frac{P_s}{P_{crit}} \right)^{-0.437}$ $h_{fc} = (1 + 1.3 X_{tt}^{-1}) h_l$ $h_l = 0.023 \left(\frac{k_l}{d} \right) Re_1^{0.8} Pr_1^{0.4}$ $h_{lf} = \beta \frac{k_1}{\delta_c}$ $\beta = \frac{x}{x + (1-x)\rho_v/\rho_l}$ $Ca = \frac{\mu_l G}{\sigma} \left(\frac{x}{\rho_v} + \frac{1-x}{\rho_l} \right)$ $\frac{\delta_c}{D_h} = 0.014 Ca^{0.1} \quad \text{for annular and churn flow}$ $h_{lf} = F_{dp} \left(\beta \frac{k_1}{\delta_c} \right)$ $\frac{\delta_c}{D_h} = 0.005 Ca^{0.05} (\rho_v/\rho_l)^{0.2}$ $F_{dp} = \min \left[7.8 Co^{-0.1} \left(\frac{q}{G \Delta h_{lv}} \times 10^4 \right)^{-0.3} \left(\frac{\rho_v}{\rho_l} \right)^{0.2} \left(\frac{G D_h}{\mu_l} \right)^{-0.16}, 1 \right]$	D _h = 0.82 mm Working fluid: R32 and R1234ze(E)

Acknowledgements This work was supported by a National Research Foundation of Korea (NRF) Grant funded by the Korean government (MIST) (No. NRF-2020R1A2C1010902). We would like to thank Essayreview www.essayreview.co.kr for the English language editing.

References

- Chen JC. Correlation for boiling heat transfer to saturated fluids in convective flow. *Ind Eng Chem Process Des Dev.* 1966;5(3):322–9. <https://doi.org/10.1021/i260019a023>.
- Gungor KE, Winterton RHS. A general correlation for flow boiling in tubes and annuli. *Int J Heat Mass Transf.* 1986;29(3):351–8. [https://doi.org/10.1016/0017-9310\(86\)90205-X](https://doi.org/10.1016/0017-9310(86)90205-X).
- Jung DS, McLinden M, Radermacher R, Didion D. A study of flow boiling heat transfer with refrigerant mixtures. *Int J Heat Mass Transf.* 1989;32(9):1751–64. [https://doi.org/10.1016/0017-9310\(89\)90057-4](https://doi.org/10.1016/0017-9310(89)90057-4).
- Mahmoud MM, Karayiannis TG. Heat transfer correlation for flow boiling in small to micro tubes. *Int J Heat Mass Transf.* 2013;66:553–74. <https://doi.org/10.1016/j.ijheatmasstransfer.2013.07.042>.
- Li M, Dang C, Hihara E. Flow boiling heat transfer of HFO1234yf and HFC32 refrigerant mixtures in a smooth horizontal tube: part

- II. Prediction method. *Int J Heat Mass Transf.* 2013;64:591–608. <https://doi.org/10.1016/j.ijheatmasstransfer.2013.04.047>.
6. Kutateladze SS. Boiling heat transfer. *Int J Heat Mass Transf.* 1961;4:31–45. [https://doi.org/10.1016/0017-9310\(61\)90059-X](https://doi.org/10.1016/0017-9310(61)90059-X).
 7. Liu Z, Winterton RHS. A general correlation for saturated and subcooled flow boiling in tubes and annuli, based on a nucleate pool boiling equation. *Int J Heat Mass Transf.* 1991;34(11):2759–66. [https://doi.org/10.1016/0017-9310\(91\)90234-6](https://doi.org/10.1016/0017-9310(91)90234-6).
 8. Steiner D, Taborek J. Flow boiling heat transfer in vertical tubes correlated by an asymptotic model. *Heat Transf Eng.* 1992;13(2):43–69. <https://doi.org/10.1080/01457639208939774>.
 9. Wattelet JP, Chato JC, Souza AL, Christoffersen BR. Evaporative characteristics of R-134a, MP-39, and R-12 at low mass fluxes. *ASHRAE Transactions.* 1994;100(1):603–615.
 10. Sempértegui-Tapia DF, Ribatski G. Flow boiling heat transfer of R134a and low GWP refrigerants in a horizontal micro-scale channel. *Int J Heat Mass Transf.* 2017;108:2417–32. <https://doi.org/10.1016/j.ijheatmasstransfer.2017.01.036>.
 11. Kattan N, Thome JR, Favrat D. Flow boiling in horizontal tubes: part 3—development of a new heat transfer model based on flow pattern. *J Heat Transf.* 1998;120(1):156. <https://doi.org/10.1115/1.2830039>.
 12. Thome JR, El Hajal J. Flow boiling heat transfer to carbon dioxide: general prediction method. *Int J Refrig.* 2004;27(3):294–301. <https://doi.org/10.1016/j.jrefrig.2003.08.003>.
 13. Yoon SH, Cho ES, Hwang YW, Kim MS, Min K, Kim Y. Characteristics of evaporative heat transfer and pressure drop of carbon dioxide and correlation development. *Int J Refrig.* 2004;27(2):111–9. <https://doi.org/10.1016/j.jrefrig.2003.08.006>.
 14. Jige D, Kikuchi S, Eda H, Inoue N. Flow boiling in horizontal multiport tube: development of new heat transfer model for rectangular minichannels. *Int J Heat Mass Transf.* 2019;144:118668. <https://doi.org/10.1016/j.ijheatmasstransfer.2019.118668>.
 15. Aghdam HH, Heravi EJ. Guide to convolutional neural network: a practical application to traffic-sign detection and classification. Berlin: Springer; 2017. p. 71–8.
 16. Priddy KL, Keller PE. Artificial neural network: an introduction. Washington: SPIE Press; 2005. p. 145–8.
 17. Thibault J, Grandjean BPA. A neural network methodology for heat transfer data analysis. *Int J Heat Mass Transf.* 1991;34(8):2063–70. [https://doi.org/10.1016/0017-9310\(91\)90217-3](https://doi.org/10.1016/0017-9310(91)90217-3).
 18. Qiu Y, Garg D, Kim SM, Mudawar I, Kharangate CR. Machine learning algorithms to predict flow boiling pressure drop in mini/micro-channels based on universal consolidated data. *Int J Heat Mass Transf.* 2021;178:121607. <https://doi.org/10.1016/j.ijheatmasstransfer.2021.121607>.
 19. Hughes MT, Fronk BM, Garimella S. Universal condensation heat transfer and pressure drop model and the role of machine learning techniques to improve predictive capabilities. *Int J Heat Mass Transf.* 2021;179:121712. <https://doi.org/10.1016/j.ijheatmasstransfer.2021.121712>.
 20. Zhou L, Garg D, Qiu Y, Kim SM, Mudawar I, Kharangate CR. Machine learning algorithms to predict flow condensation heat transfer coefficient in mini/micro-channel utilizing universal data. *Int J Heat Mass Transf.* 2020;162:20351. <https://doi.org/10.1016/j.ijheatmasstransfer.2020.120351>.
 21. Zhu G, Wen T, Zhang D. Machine learning based approach for the prediction of flow boiling/condensation heat transfer performance in mini channels with serrated fins. *Int J Heat Mass Transf.* 2021;166:120783. <https://doi.org/10.1016/j.ijheatmasstransfer.2020.120783>.
 22. Kuang Y, Han F, Sun L, Zhuan R, Wang W. Saturated hydrogen nucleate flow boiling heat transfer coefficients study based on artificial neural network. *Int J Heat Mass Transf.* 2021;175:121406. <https://doi.org/10.1016/j.ijheatmasstransfer.2021.121406>.
 23. Goodfellow I, Bengio Y, Courville A. Deep learning. Cambridge: The MIT Press; 2016.
 24. Chien NB, Choi KI, Oh JT, Cho H. An experimental investigation of flow boiling heat transfer coefficient and pressure drop of R410A in various minichannel multiport tubes. *Int J Heat Mass Transf.* 2018;127:675–86. <https://doi.org/10.1016/j.ijheatmasstransfer.2018.06.145>.
 25. Pham QV, Oh JT. Condensation heat transfer characteristics of R1234yf inside multiport mini-channel tube. *Int J Heat Mass Transf.* 2021; 121029. <https://doi.org/10.1016/j.ijheatmasstransfer.2021.121029>.
 26. Hoang HN, Agustiarini N, Oh JT. Experimental investigation of two-phase flow boiling heat transfer coefficient and pressure drop of R448A inside multiport mini-channel tube. *Energies* 2022;15(12):4331. <https://doi.org/10.3390/en15124331>.
 27. ISO GUM. Guide to the expression of uncertainty in measurement, first ed., 1993, corrected and reprinted, 1995. International Organization for Standardization, Geneva, 1995.
 28. Zhu Y, Wu X, Zhao R. R32 flow boiling in horizontal mini channels: part I. Two-phase flow patterns. *Int J Heat Mass Transf.* 2017;115:1223–32. <https://doi.org/10.1016/j.ijheatmasstransfer.2017.07.101>.
 29. He G, Zhou S, Li D, Cai D, Zou S. Experimental study on the flow boiling heat transfer characteristics of R32 in horizontal tubes. *Int J Heat Mass Transf.* 2018;125:943–58. <https://doi.org/10.1016/j.ijheatmasstransfer.2018.04.116>.
 30. Jige D, Kikuchi S, Mikajiri N, Inoue N. Flow boiling heat transfer of zeotropic mixture R1234yf/R32 inside a horizontal multiport tube. *Int J Refrig.* 2020;19:390–400. <https://doi.org/10.1016/j.jrefrig.2020.04.036>.
 31. Bertsch SS, Groll EA, Garimella SV. A composite heat transfer correlation for saturated flow boiling in small channels. *Int J Heat Mass Transf.* 2009;52(7–8):2110–8. <https://doi.org/10.1016/j.ijheatmasstransfer.2008.10.022>.
 32. D.P. Kingma, J.L. Ba, Adam: A method for stochastic optimization, *Int Conf on Learning Representations.* 2015
 33. Nettleton D. Commercial data mining: Processing, analysis, and modeling for predictive analytics projects. Elsevier Inc. 2014. pp. 84.
 34. Prieto A, Prieto B, Ortigosa EM, Ros E, Pelayo F, Ortega J, Rojas I. Neural networks: an overview of early research, current frameworks and new challenges. *Neurocomputing.* 2016;214:242–68. <https://doi.org/10.1016/j.neucom.2016.06.014>.

Publisher's Note Springer Nature remains neutral with regard to jurisdictional claims in published maps and institutional affiliations.

Springer Nature or its licensor (e.g. a society or other partner) holds exclusive rights to this article under a publishing agreement with the author(s) or other rightsholder(s); author self-archiving of the accepted manuscript version of this article is solely governed by the terms of such publishing agreement and applicable law.